CONTROLAR: CONTROLLABLE IMAGE GENERATION WITH AUTOREGRESSIVE MODELS

Zongming Li[1][*]**, Tianheng Cheng**[1][*]**, Shoufa Chen**[2]**, Peize Sun**[2]**, Haocheng Shen**[3]**,**
Longjin Ran[3]**, Xiaoxin Chen**[3]**, Wenyu Liu**[1] **& Xinggang Wang**[1][†]

[1] School of EIC, Huazhong University of Science and Technology
[2] Department of Computer Science, The University of Hong Kong
[3] vivo AI Lab

ABSTRACT

Autoregressive (AR) models have reformulated image generation as *next-token prediction*, demonstrating remarkable potential and emerging as strong competitors to diffusion models. However, control-to-image generation, akin to ControlNet, remains largely unexplored within AR models. Although a natural approach, inspired by advancements Large Language Models, is to tokenize control images into tokens and prefill them into the autoregressive model before decoding image tokens, it still falls short in generation quality compared to ControlNet and suffers from inefficiency. To this end, we introduce ControlAR, an efficient and effective framework for integrating spatial controls into autoregressive image generation models. Firstly, we explore control encoding for AR models and propose a lightweight control encoder to transform spatial inputs (*e.g.*, canny edges or depth maps) into control tokens. Then ControlAR exploits the *conditional decoding* method to generate the next image token conditioned on the per-token fusion between control and image tokens, similar to positional encodings. Compared to prefilling tokens, using conditional decoding significantly strengthens the control capability of AR models but also maintains the model efficiency. Furthermore, the proposed ControlAR surprisingly empowers AR models with arbitrary-resolution image generation via conditional decoding and the specific controls. Extensive experiments can demonstrate the controllability of the proposed ControlAR for the autoregressive control-to-image generation across diverse inputs, including edges, depths, and segmentation masks. Furthermore, both quantitative and qualitative results indicate that ControlAR surpasses previous state-of-the-art controllable diffusion models, *e.g.*, ControlNet++. The code, models, and demo will soon be available at https://github.com/hustvl/ControlAR.
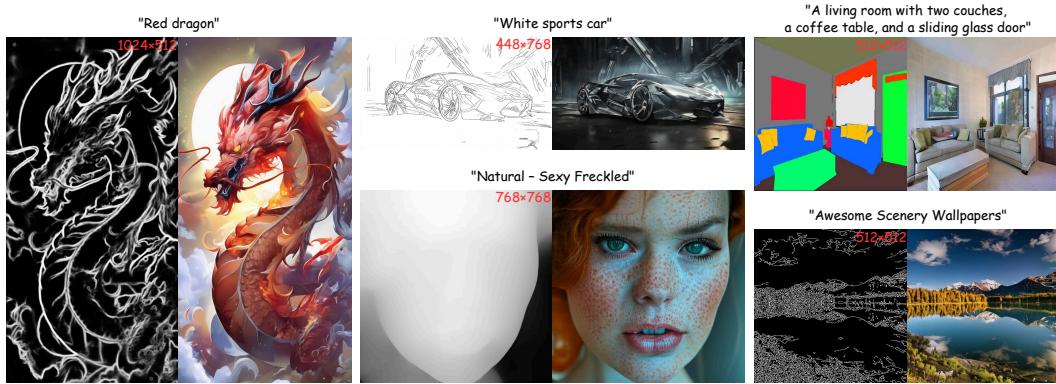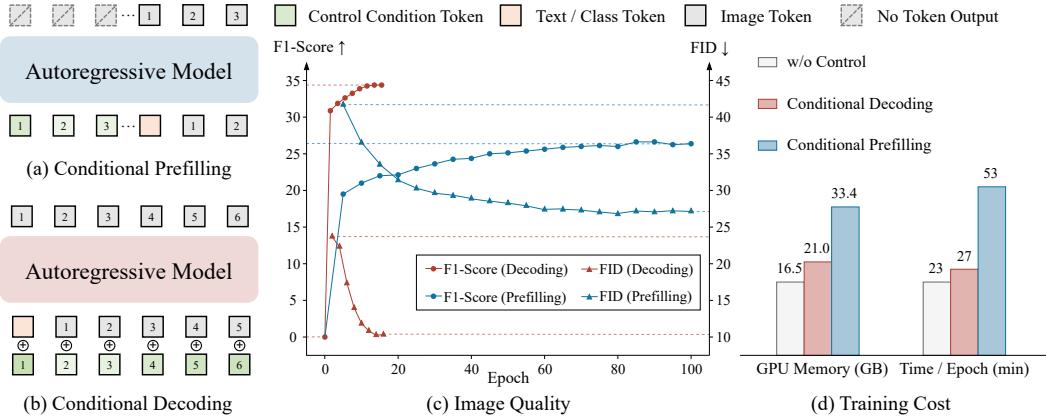
Figure 1: **Arbitrary-resolution images generated by ControlAR.** Our ControlAR extends autoregressive models, *e.g.*, LlamaGen (Sun et al., 2024), to generate high-quality images using spatial controls and expands the capability of autoregressive models to any-resolution image generation.

Figure 2: **Comparison between Conditional Prefilling *v.s.* Conditional Decoding.** We encode the spatial control images into a sequence of control tokens for autoregressive models. (a) Conditional Prefilling: control condition tokens are prefilled into the autoregressive model before the first image token is generated. (b) Conditional Decoding: each image token is fused with the control condition token to predict the next image token. (c) Image Quality: we compare the performance (*i.e.*, F1-Score and FID) across training epochs between conditional decoding and prefilling. It's remarkable that conditional decoding outperforms conditional prefilling in terms of performance and training convergence speed. (d) Training cost: conditional prefilling significantly increases the training memory (+59.1%) and training latency (+96.3%) compared to conditional decoding.

1 INTRODUCTION

[1] [2] Recent advancements in image generation have led to the emergence of various models that leverage text-to-image diffusion models (Saharia et al., 2022; Ho et al., 2022; Rombach et al., 2022; Podell et al., 2023) to generate high-quality visual content. Among them, several works (Zhang et al., 2023a; Li et al., 2024b; Qin et al., 2023b) such as ControlNet (Zhang et al., 2023a), have explored adding conditional controls to text-to-image diffusion models and allowed for image generation according to the precise spatial controls, *e.g.*, edges, depth maps, or segmentation masks. The control-to-image diffusion models have impressively enhanced the versatility of these models in applications ranging from creative design to augmented reality.

Despite the success of diffusion models, most recent works reveal the potential of autoregressive models for image generation, *e.g.*, LlamaGen (Sun et al., 2024) follows the architecture of Llama (Touvron et al., 2023) to achieve image generation and obtained remarkable results. Moreover, several works (Kondratyuk et al., 2024; Gao et al., 2024) have explored autoregressive models for video generation and achieved promising results, further demonstrating the great potential of autoregressive models for visual generation. However, controlling autoregressive models as a crucial direction remains unexplored, making it challenging for autoregressive models to achieve same level of fine-grained control as diffusion models. In contrast to controllable diffusion models, adding conditional controls to autoregressive models is not straightforward because of two major challenges: (1) *how to encode 2D spatial control images for autoregressive models* and (2) *how to guide image generation with encoded controls*. Specifically, diffusion models directly use the 2D features of control images and control the generated image through pixel-wise feature fusion. However, autoregressive models adopt sequence modeling and next-token prediction to perform image generation sequentially. Therefore, the techniques proposed in (Zhang et al., 2023a; Li et al., 2024b) are infeasible in autoregressive models.

In this paper, we delve into the two aforementioned challenges and introduce the **Control**lable **A**uto**R**egressive (ControlAR) framework to enhance the control capabilities of autoregressive image generation models such as LlamaGen (Sun et al., 2024) or AiM (Li et al., 2024a). Firstly, we propose a control encoder to obtain sequential encodings of control images and output the control tokens, which are more suitable than 2D control features for autoregressive models. Instead of

---

[1]Equal contribution. Works was done during Zongming Li's internship at vivo AI Lab.
[2]Corresponding author (`xgwang@hust.edu.cn`).

directly replicating the modules of diffusion models for control feature extraction, we use a Vision Transformer (ViT) as the encoder and further investigate the most effective ViT pre-training scheme, *e.g.*, vanilla (Dosovitskiy, 2020) or self-supervised (Oquab et al., 2023) for encoding spatial controls towards image generation. Secondly, we naturally consider that directly prefilling control tokens, inspired by Large Language Models and prompt techniques (Pope et al., 2023), can provide a simple and effective autoregressive control approach, as shown in Fig. 2 (a). However, it struggles to achieve satisfactory results, *i.e.*, the LlamaGen with conditional prefilling obtains 26.45 FID with the Canny edge control on ImageNet, which is much inferior to ControlNet (10.85 FID). Moreover, it tends to increase sequence length, inevitably raising the cost of training and inference. To remedy the above issues, we formulate controllable autoregressive generation as *conditional decoding*, in which predicting the next image token is conditioned on both the previous image token and the current control token, as shown in Fig. 2 (b). Specifically, the input image token is fused with the corresponding control token and fed into the model for the next-token prediction. The proposed ControlAR leverage the conditional decoding strategy in several intermediate layers of the AR model to maintain control information across decoding layers. Fig. 2 (c) indicates that the proposed conditional decoding clearly surpasses the well-known conditional prefilling in terms of both the image quality (FID) and control capability (F1-Score). In addition, the proposed conditional decoding, without increasing the sequence length, brings negligible computation costs on the original autoregressive model, as shown in Fig. 2 (d), demonstrating superiority compared to conditional prefilling.

Most importantly, ControlAR surprisingly provides an effective way to control the resolution (size and aspect ratio) of image generation, allowing autoregressive models to get rid of the constraints of generating images at a fixed resolution, *e.g.*, LlamaGen (Sun et al., 2024) can only generate images of 256×256 after trained on 256×256 images. By adjusting the input size of the control, ControlAR decodes image tokens according to the sequence of control tokens, making it easy to achieve any-resolution image generation without resolution-aware prompts (Liu et al., 2024). In addition, we propose the multi-resolution ControlAR with multi-scale training to further enhance the image quality of different resolutions, as shown in Fig. 1.

Quantitative and qualitative experiments demonstrate that ControlAR can obtain better performance compared to previous state-of-the-art methods based on well-established diffusion models towards diverse controllable image generation. Especially, the experiments also showcase the zero-shot or fine-tuned ability to control any-resolution image generation and prove the effects of ControlAR.

The main contribution of this paper can be summarized as follows:

- We explore controllable autoregressive image generation and present ControlAR, which enables precise control and generates high-quality images. ControlAR exploits the control encoder to transform the control images into a sequence of conditional tokens and adopt the proposed conditional decoding to predict the next image token conditioned on the control and image tokens, which proves more effective than conditional prefilling.

- The proposed ControlAR easily expands autoregressive models with strong control capability. Under various control conditions, the proposed ControlAR demonstrates its highly competitive performance towards conditional consistency and image quality compared to state-of-the-art diffusion methods, *e.g.*, ControlNet++.

- We exploit the properties of our proposed conditional decoding to extend the ability of the autoregressive model to generate arbitrary resolution. With a simple multi-resolution training recipe, , we extend ControlAR to Multi-Resolution ControlAR (MR-ControlAR), which allows autoregressive models to generate high-quality images with different resolutions, further enhancing their control capability.

2 RELATED WORK

2.1 IMAGE GENERATION WITH DIFFUSION MODELS

Diffusion models (Song & Ermon, 2019; Ho et al., 2020; Song et al., 2020a; Dhariwal & Nichol, 2021; Nichol et al., 2021; Lu et al., 2022; Rombach et al., 2022; Podell et al., 2023) have cemented their status as a dominant paradigm in generative modeling, especially in the domain of image synthesis. They employ an iterative denoising process to create images from Gaussian noise. Since the

introduction of the diffusion model (Sohl-Dickstein et al., 2015), subsequent research has focused on refining training and sampling strategies (Song et al., 2020b; Ho et al., 2020; Song et al., 2020a). Simultaneously, in an effort to reduce computational complexity in the image generation process and enhance efficiency, numerous studies have sought to translate the generation process into the latent space (Rombach et al., 2022; Podell et al., 2023; Esser et al., 2024). Within the realm of text-to-image generation, the prevailing framework involves utilizing U-Net (Ronneberger et al., 2015) as the denoising network, while leveraging pre-trained CLIP (Radford et al., 2021) or T5 (Raffel et al., 2020) as the text encoder to extract textual features and integrate them into the denoising process through the cross-attention mechanism. Furthermore, DiT (Peebles & Xie, 2023) employs Transformer (Vaswani, 2017) as the denoising network, yielding highly competitive results in image generation. Despite the considerable progress in diffusion models, the field of image generation still trails behind the advancement of large language models based on autoregressive mechanisms.

2.2 IMAGE GENERATION WITH AUTOREGRESSIVE MODELS

In contrast to the iterative denoising process of the diffusion model, the autoregressive model operates on the principle of predicting the next image token based on the existing image tokens. Early autoregressive image generation models (Van Den Oord et al., 2016; Van den Oord et al., 2016) focused on predicting individual pixel values. Subsequent approaches (Esser et al., 2021; Ramesh et al., 2021; Yu et al., 2022) attempt to use an image tokenizer to convert continuous images into discrete tokens. More recently, there has been a growing trend towards leveraging efficient language model architectures as generative networks for autoregressive image generation. LlamaGen (Sun et al., 2024) and Open-MAGVIT2 (Luo et al., 2024) use the Llama architecture (Touvron et al., 2023) as the generative network, demonstrating its significant potential for image generation. AiM (Li et al., 2024a) explores an approach using the Mamba model (Gu & Dao, 2023) as the generative network. Lumina-mGPT (Liu et al., 2024) develops a family of multimodal autoregressive models capable of a wide range of visual and linguistic tasks, particularly excelling in generating flexible, photorealistic images from textual descriptions. In addition, some recent works (Xie et al., 2024; Zhou et al., 2024) fuse autoregressive and diffusion into one multi-modal model for simultaneous image generation and understanding.

2.3 CONTROLLABLE IMAGE GENERATION

Relying solely on textual prompts is insufficient for conveying distinctive artistic style or precise detail during T2I image generation. Some methods (Gal et al., 2022; Ruiz et al., 2023; Zhang et al., 2023b) attempt to capture concepts from example images that are not easily described through text to guide image generation, a task known as personalization for controllable generation. Represented by ControlNet (Zhang et al., 2023a) and T2I-Adapter (Mou et al., 2024), work in this area utilizes the spatial structure of the image, such as edges, segmentation masks, depth maps, etc., to enable spatial control in the generation process. Subsequently, UniControl (Qin et al., 2023b), Uni-ControlNet (Zhao et al., 2024), and ControlNet++ (Li et al., 2024b) further extend this realm, focusing on condition encoder design and optimization of training strategies. Furthermore, Glue-Gen (Qin et al., 2023a) pairs a multi-modal encoder with a stable diffusion model for sound-to-image generation. Controllable generation based on autoregressive image generation models has been less explored. ControlVAR (Li et al., 2024c) employs next-scale prediction to jointly model control and image, but is still different from next-token prediction in autoregressive generation. Our objective is to fully harness the capabilities of autoregressive models and explore a general and efficient paradigm for controllable image generation using autoregressive models.

3 CONTROLAR

3.1 PRELIMINARY: IMAGE GENERATION WITH AUTOREGRESSIVE MODELS

Autoregressive models define the generative process as *next-token prediction*:

$$p(\mathbf{x}) = \prod_{i=1}^{n} p(x_i|x_1, x_2, \ldots, x_{i-1}) = \prod_{i=1}^{n} p(x_i|x_{<i}), \tag{1}$$

and when performing image generation, x_i in Eq. 1 represents the image token. The latest autoregressive image generation models such as LlamaGen (Sun et al., 2024) and AiM (Li et al., 2024a) use vector quantization to convert compressed image patches into discrete image tokens. The process of image generation is formulated as follows:

$$p(\mathbf{q}) = \prod_{t=1}^{h \cdot w} p(q_t | q_{<t}, c), \qquad (2)$$

where q_t is the discretised image token, c is class label embedding or text embedding, and $h \cdot w$ is the total number of image tokens. During training, these two methods use causal Transformer (Vaswani, 2017) and Mamba (Gu & Dao, 2023) to model the sequence respectively, with the aim of minimising the prediction loss of the next image token, which can be written as follows:

$$\mathcal{L}_{train} = \boldsymbol{CE}(\mathbf{M}([c, q_1, q_2, \ldots, q_{l-1}]), [q_1, q_2, \ldots, q_l]), \qquad (3)$$

where $\boldsymbol{CE}$ denotes cross-entropy loss, $\mathbf{M}$ denotes the sequence model, and l is the sequence length.

3.2 Unified Conditional Decoding

Autoregressive image generation models leverage the two-phase generation process, including the prefilling and decoding (Pope et al., 2023; Kwon et al., 2023), where prefilling processes the prompt tokens (or control tokens) and stores them in the KV Cache (Pope et al., 2023), and then decoding follows next-token prediction and aims to generate the output tokens (*e.g.*, image tokens). In ControlAR, we bring the condition into the decoding phase by adding the control condition token to the image token, which we refer to as conditional decoding. Specifically, modify Eq. 2 as follows:

$$p(\mathbf{q}) = \prod_{t=1}^{h \cdot w} p(q_t | q_1 + C_2, q_2 + C_3, \ldots, q_{t-1} + C_t, c + C_1), \qquad (4)$$

where C represents the control condition token generated from the control image. The number of control condition tokens is the same as the number of image tokens expected to be generated. It is worth noting that we use displacement by one position when adding the control condition tokens to the sequence, which allows the model to make autoregressive predictions with control information corresponding to the next image token.

Conditional decoding avoids the network having to learn the positional correspondence between the condition signal and the image, as the positional information is fixed into the sequence during the fusion of the control condition tokens. Additionally, the computational increase of this approach to the generation process is minimal. Inputting conditional signals by prefilling additional tokens will result in a significant increase in computational complexity, especially when the computational complexity of the sequence model is quadratic to the length of the sequence, as in the case of the Transformer (Vaswani, 2017). The results in Fig. 2 (d) demonstrate this.

3.3 Controllable Autoregressive Model

Overall architecture. In our ControlAR framework shown in Fig. 3, controllable generation occurs in two main steps. First, we employ a control encoder to extract features from the control images, such as hed edges, to generate a control condition sequence of length L, as depicted in Fig. 3 (a). The second step involves integrating the control condition tokens into the autoregressive image generation process, as shown in Fig. 3 (b). To achieve this, we expand the sequence layer (*e.g.*, causal Transformer layer or Mamba layer) of the autoregressive model to *conditional sequence layer* by directly adding the control condition tokens to the image tokens based on positional correspondence, as discussed in Sec. 3.2. Specifically, we adopt a MLP to project the control tokens and then fuse them with image tokens via the simple addition. Furthermore, to strengthen the control of the conditions over the generated images, we evenly replace the conditional sequence layer three times in the autoregressive model. Throughout the training process of our ControlAR, we update the parameters of the sequence model, thereby enhancing the model's capability for stronger and more controllable image generation.

Control encoder. We propose a lightweight control encoder to transform control image to control condition tokens. In contrast to previous approaches such as ControlNet (Zhang et al., 2023a) and T2I-Adapter (Mou et al., 2024), we utilize the Vision Transformer (ViT) (Dosovitskiy, 2020) for feature extraction of control images. We believe that a ViT model, pre-trained on a large amount of data, is more adept at modeling sequences than a randomly initialized CNN network. For the class-to-image task on ImageNet, we use ViT-S to initialize our control encoder. Additionally, for the text-to-image task, we employ DINOv2-S (Oquab et al., 2023) as the initialization scheme for the control encoder. Further details on this are available in section 4.3. Notably, our ControlAR achieves efficient controllable generation with a control encoder comprising only about 22M parameters, which is significantly less than the 361M parameter count of ControlNet++.

3.4 AUTOREGRESSIVE ARBITRARY-RESOLUTION GENERATION.

Benefiting from the proposed conditional decoding, which generates the next image token conditioned on the current control token and the number of image tokens aligns with the control tokens. Therefore, we can directly adjust the resolutions of generated images according to the length of the control tokens, allowing the autoregressive models to generate arbitrary-resolution images. Rather than resizing the control images into a fixed resolution, *e.g.*, 512×512, we can directly input the control images with original resolutions into ControlAR to obtain the generated images. To further enhance the image quality of arbitrary-resolution image generation, we adopt a multi-resolution training recipe, which randomly samples different resolutions, and present the Multi-Resolution ControlAR (MR-ControlAR). Without extra modules or parameters, our MR-ControlAR is capable of generating image of arbitrary resolutions without significant quality degradation, thereby further expanding the versatility of autoregressive models.

Figure 3: **The overall architecture of ControlAR**. The control image will be flattened into patches and encoded as a sequence of control tokens via the proposed **control encoder**. For controllable image generation, we extend several sequential layers (*i.e.*, causal Transformer layer or Mamba layer) of the autoregressive model into **conditional sequential layers** by incorporating the fusion of control tokens and image tokens to predict the next image token. Finally, the image tokens are decoded into a generated image through the VQGAN decoder.

4 EXPERIMENTS

4.1 EXPERIMENTAL SETUP

Datasets. Our experiments are divided into two main parts: class-to-image (C2I) and text-to-image (T2I) controllable generation. For the former, we follow ControlNet (Zhang et al., 2023a) to extract the canny edges and depth maps of the images in ImageNet (Deng et al., 2009) for training. In T2I experiments, we train controllable generation for segmentation masks, canny edges, hed edges, lineart edges, and depth maps. For segmentation masks, we use ADE20K (Zhou et al., 2017) and CO-COStuff (Caesar et al., 2018) as training data, with the text captions sourced from ControlNet++ (Li et al., 2024b), which adopts MiniGPT-4 (Zhu et al., 2023) to obtain a short description of the image. Furthermore, we use a subset of LAION-Aesthetics (Schuhmann et al., 2022), MultiGen-20M (Qin et al., 2023b), as the training data for canny edge, hed edge, lineart edge, and depth map controllable generation. Additional details are provided in the supplementary material.

Evaluation and metrics. We train the proposed ControlAR for different controllable generation tasks on several datasets and evaluate them using the corresponding validation datasets. We mainly employ two metrics: conditional consistency and Fréchet Inception Distance (FID) (Heusel et al.,

Table 1: **C2I controllable generation.** Param. denotes the number of parameters of the C2I model. "↑" or "↓" indicate lower or higher values are better. "*" indicates that ControlVAR's FID values are estimated from its histograms (Li et al., 2024c). The results are conducted on 256×256 resolution.

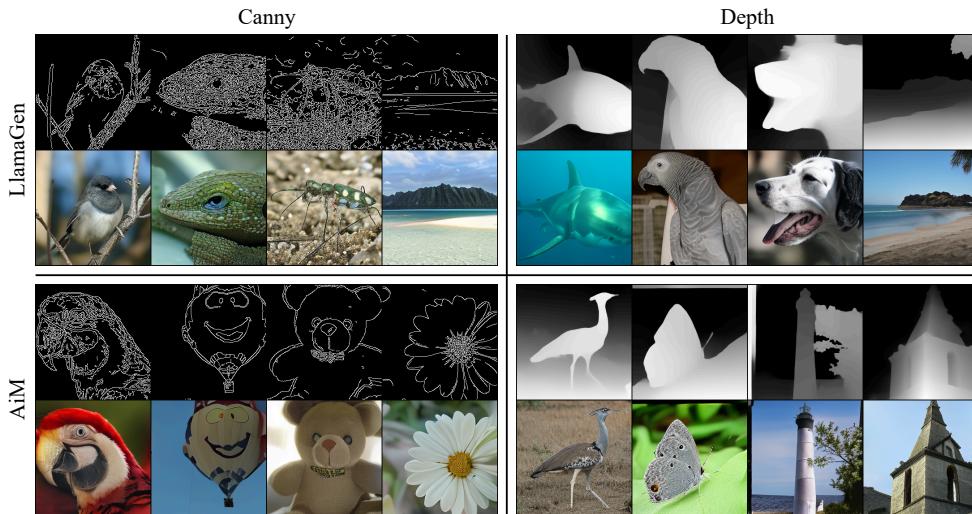| Method | C2I Model | Param. | Canny | | Depth | |
			F1-Score ↑	FID ↓	RMSE ↓	FID ↓
ControlVAR*	VAR-d16	310M	-	16.20	-	13.80
	VAR-d20	600M	-	13.00	-	13.40
	VAR-d24	1.0B	-	15.70	-	12.50
	VAR-d30	2.0B	-	7.85	-	6.50
Ours	AiM-L	350M	30.36	9.66	35.01	7.39
	LlamaGen-B	111M	34.15	10.64	32.41	6.67
	LlamaGen-L	343M	34.91	7.69	31.11	4.19

Figure 4: **Visualization of C2I controllable generation.** Our ControlAR generates images with high conditional consistency and quality on both LlamaGen and AiM.

2017). We evaluate the conditional consistency by calculating the similarity between the input condition images and the extracted condition images from the generated images. When evaluating segmentation masks control, we use a segmentation method, *i.e.*, Mask2Former (Cheng et al., 2022), to compute the mean Intersection-over-Union (mIoU) on generated images. We adopt the F1-Score and Root Mean Square Error (RMSE) to evaluate the similarity of canny edges and depth maps, respectively. Additionally, for hed edge and lineart edge, we utilize SSIM as the metric. Alongside these quantitative metrics, we provide abundant qualitative visualizations on diverse controls.

Implementation details. In C2I controllable generation experiments, we employ LlamaGen (Sun et al., 2024) and AiM (Li et al., 2024a) as the foundational autoregressive models for ControlAR. During the fine-tuning on ImageNet (Deng et al., 2009), we adopt the AdamW optimizer (Kingma, 2014). The learning rate is set to 1e-4 and 8e-4 for training LlamaGen and AiM respectively. We use the image size of 256×256, with a batch size of 256 for canny edge and depth maps. In T2I experiments, we mainly use LlamaGen-XL, which is built upon a T5 encoder (Raffel et al., 2020) and contains 775M parameters. We employ the AdamW optimizer with a learning rate of 5e-5 and resize both input and control images to 512×512 for comparison with other methods.

4.2 EXPERIMENTAL RESULTS

C2I controllable generation. We utilize the ImageNet (Deng et al., 2009) to conduct controllable generation experiments for C2I, and the results are shown in Tab. 1. We calculate the conditional consistency (F1-Score or RMSE) and the FID of the images generated by ControlAR and compare the FID with ControlVAR (Li et al., 2024c). It shows that our proposed ControlAR achieves

Table 2: **Conditional consistency of T2I controllable generation.** "↑" or "↓" indicate lower or higher values are better. "-" denotes that the method does not release a model for testing. The results are conducted on 512×512 resolution.

Method	Seg.	Seg.	Canny	Hed	Lineart	Depth
	mIoU ↑	mIoU ↑	F1-Score ↑	SSIM ↑	SSIM ↑	RMSE ↓
	ADE20K	COCOStuff	MultiGen-20M	MultiGen-20M	MultiGen-20M	MultiGen-20M
GLIGEN	23.78	-	26.94	-	-	38.83
T2I-Adapter	12.61	-	23.65	-	-	48.40
Uni-ControlNet	19.39	-	27.32	69.10	-	40.65
UniControl	25.44	-	30.82	79.69	-	39.18
ControlNet	32.55	27.46	34.65	76.21	70.54	35.90
ControlNet++	**43.64**	34.56	37.04	80.97	**83.99**	**28.32**
Ours	39.95	**37.49**	**37.08**	**85.63**	79.22	29.01

Table 3: **FID of T2I controllable generation.** "-" denotes that the method does not release a model for testing. Our ControlAR achieves significant FID improvements.

Method	Seg.	Seg.	Canny	Hed	Lineart	Depth
	ADE20K	COCOStuff	MultiGen-20M	MultiGen-20M	MultiGen-20M	MultiGen-20M
GLIGEN	33.02	-	18.89	-	-	18.36
T2I-Adapter	39.15	-	15.96	-	-	22.52
Uni-ControlNet	39.70	-	17.14	17.08	-	20.27
UniControl	46.34	-	19.94	15.99	-	18.66
ControlNet	33.28	21.33	**14.73**	15.41	17.44	17.76
ControlNet++	29.49	19.29	18.23	15.01	13.88	16.66
Ours	**27.15**	**14.51**	17.51	**10.53**	**12.41**	**14.61**

lower FID based on the LlamaGen-L, which only has 16.7% of parameters of VAR-d30 (Tian et al., 2024). In addition, the experimental results show that our method achieves good results with different autoregressive models including Transformer-based LlamaGen and Mamba-based AiM. Fig. 4 illustrates the visualizations of ControlAR with different autoregressive models.

T2I controllable generation.   We mainly employ LlamaGen-XL as the autoregressive model for T2I generation. Tab. 2 presents the quantitative comparison of controllability with state-of-the-art methods. Among those methods in Tab. 2, GLIGEN (Li et al., 2023) utilizes SD1.4 (Rombach et al., 2022) as the generative model, while T2I-Adapter (Mou et al., 2024), Uni-ControlNet (Zhao et al., 2024), UniControl (Qin et al., 2023b), ControlNet (Zhang et al., 2023a), and ControlNet++ (Li et al., 2024b) adopt SD1.5 (Rombach et al., 2022) as the generative model. As Tab. 2 shows, it is evident that our ControlAR is highly competitive compared to the existing diffusion-based methods. The proposed ControlAR significantly outperforms ControlNet (Zhang et al., 2023a) in terms of diverse control tasks. Compared to ControlNet++ (Li et al., 2024b), which is fine-tuned based on the well-established ControlNet, our ControlAR demonstrates comparable or even better controlling performance, for example, achieving an improvement of 4.66 SSIM on the hed edges task. Additionally, we report the FID for the generated images in Tab. 3. Our approach attains the better FID across various tasks compared with ControlNet++, indicating that it not only possesses strong controllability but also ensures the quality of image generation. We provide qualitative comparison in Fig. 5, and more visualizations are available in the supplementary material.

Arbitrary-Resolution Generation.   Instead of uniformly resizing the controls and images to 512 $\times$ 512, we adopt a set of resolutions ranging from 384 to 1024 and keep the image sequence length to no more than 2304 to train our Multi-Resolution ControlAR. Direct end-to-end controllable generation using MR-ControlAR preserves the detailed features of the control image and avoids the loss of information due to scaling. We show the difference between these two approaches in Fig. 6 (a), and perform hed edge control generation experiments on images with different resolution ratios in the validation set of MultiGen-20M. Experimental results show that after multi-resolution training, MR-ControlAR can ensure that the generation of images with different resolution ratios is not impaired. We show the visualization at different resolutions in Fig. 1.
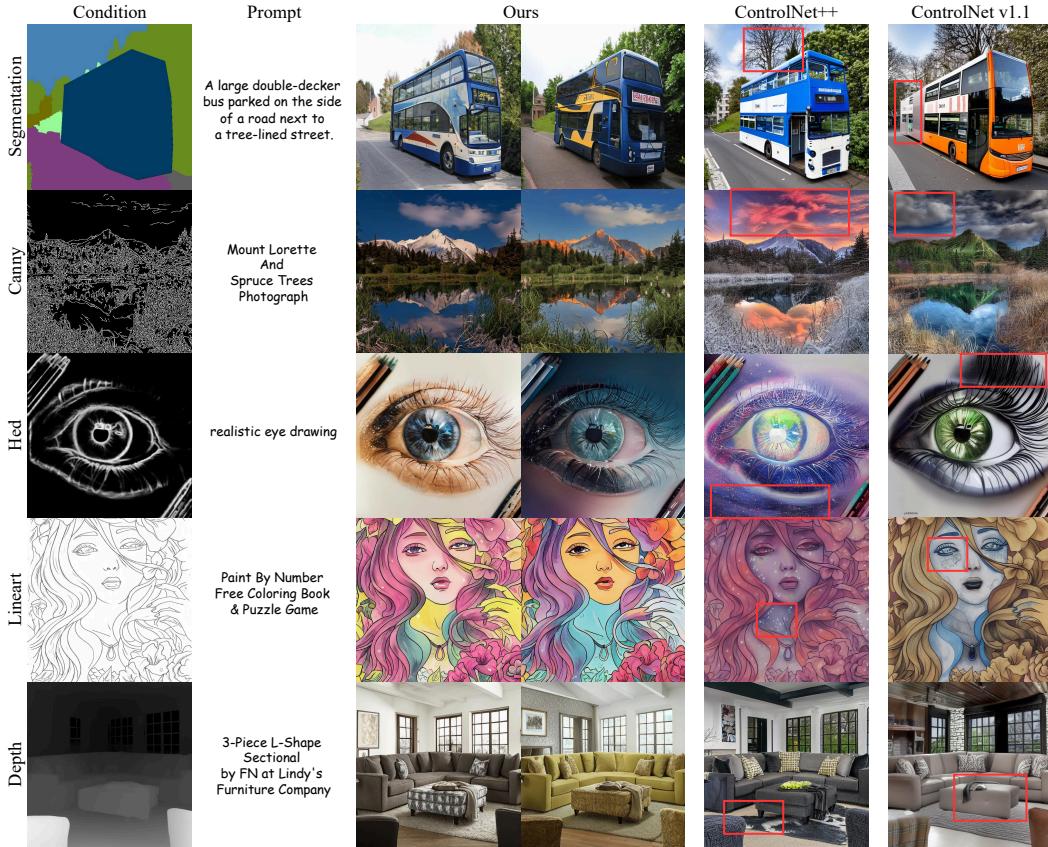
Figure 5: **Visualization of text-to-image controllable generation.** We use red boxes to mark areas where the generated results of other methods differ from the input control image.

(a) Generation process under resolution of 768×512
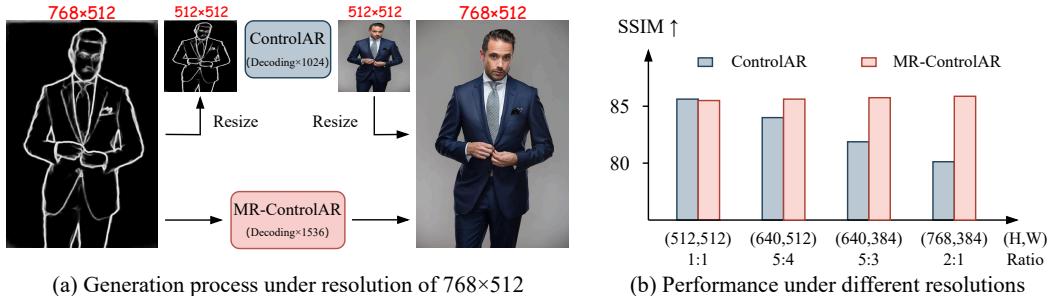
(b) Performance under different resolutions

Figure 6: **Comparison of ControlAR and Multi-Resolution ControlAR.** (a) shows the generation process of ControlAR and MR-ControlAR under the resolution of 768×512. "Decoding $\times$ 1024" denotes that 1024 image tokens need to be decoded for output. (b) compares the conditional consistency of ControlAR and MR-ControlAR under different resolutions of control conditions.

4.3 ABLATION STUDIES

Ablations on the Control Encoder. In Tab. 4, we conduct experiments using different encoders (or pre-training schemes) towards different controls, including canny edge, depth map, and hed edge. Firstly, we follow T2I-Adapter (Mou et al., 2024) and design a vanilla convolutional control encoder with 4 consecutive residual blocks (He et al., 2016) and a total downsample ratio of 16. The vanilla CNN-based control encoder contains 21.8M parameters, which has similar parameters with ViT-S (Dosovitskiy, 2020). Further, we explore the effects of using pre-trained ViTs as our control encoder and adopt ViTs with different pre-trained schemes, *i.e.*, the ImageNet-supervised (Dosovitskiy, 2020) and self-supervised (Oquab et al., 2023). For our experiments, we employ LlamaGen-B's

9

Table 4: **Ablations on the Control Encoder.** "↑" or "↓" indicate lower or higher values are better.

Control Encoder	Params	Canny (C2I)		Depth (C2I)		Hed (T2I)	
		F1-Score ↑	FID ↓	RMSE ↓	FID ↓	SSIM ↑	FID ↓
CNN (4× Res. Blocks)	21.8M	33.55	12.27	33.36	6.97	81.64	15.33
ViT-S	22.1M	**34.15**	10.64	32.41	6.64	82.37	14.59
DINOv2-S	22.1M	33.38	10.87	32.82	7.31	85.63	10.53
DINOv2-B	86.6M	34.07	**9.47**	**31.81**	**6.36**	**86.12**	**8.58**

Table 5: **Ablations on the control fusion strategy.** "↑" or "↓" indicate lower or higher values are better.

Fusion Strategy	#Layer	F1-Score ↑	FID ↓
Cross-Attention	1-th	30.86	15.34
Addition	1-th	34.01	11.02
Addition	1,5,9-th	34.15	10.64
Addition	1∼12-th	34.21	11.75

Table 6: **Ablations on the training strategy.** "↑" or "↓" indicate lower or higher values are better.

Training Strategy	F1-Score ↑	FID ↓
Freeze	30.62	13.67
LoRA	32.90	13.20
Full fine-tune	34.15	10.64

C2I model to conduct experiments on the ImageNet (Deng et al., 2009) for canny edge and depth map conditions, while using LlamaGen-XL's T2I model to carry out experiments on the MultiGen-20M (Qin et al., 2023b) for the hed edge condition. As depicted in the table, different control encoders exhibit varying performance across different datasets, with the ViT-S demonstrating superior suitability for the ImageNet dataset, and the DINOv2-S yielding better results on the MultiGen-20M dataset. Furthermore, we evaluate the performance of larger encoders such as DINOv2-B, and the outcomes reveal that higher parameter counts enable our method to achieve superior results.

Ablations on the Control Fusion Strategy.   We explore different strategies for fusing control condition tokens with image tokens using the canny edge condition on ImageNet and LlamaGen-B as the generative model. Tab. 5 shows the results. Specifically, when using cross-attention for control fusion, we assign control condition tokens as the key and value, while image tokens serve as the query. Within LlamaGen-B, consisting of 12 layers of Transformer, we conduct experiments with addition at the first layer, addition at layer 1, 5, and 9, and addition at each layer. The results indicate that direct addition proves more efficacious than cross-attention. This outcome may be due to cross-attention needing to first understand the positional relationship between the image block and the control condition token, potentially leading to slower convergence. Furthermore, augmenting the frequency of addition yields enhanced conditional coherence within the generated imagery. However, an excessive degree of addition also correlates with an increase in FID.

Ablations on Sequence Model Training Strategy.   We conduct ablation experiments on the parameter update strategy of the sequence model during training. In the field of controllable generation, the most common ways of updating the parameters of a generative model include complete freezing, updating using Low-Rank Adaptation (LoRA) (Hu et al., 2021), and full fine-tuning. The results of the experiment are displayed in Tab. 6. We use LlamaGen-B as the generative model for experiments on ImageNet based on canny edge. Experimental results show that full fine-tuning outperforms other schemes in terms of conditional consistency and FID of the generated images.

Conditional Decoding *v.s.* Conditional Prefilling.   In this part, we present a comprehensive comparison between two methods: conditional decoding and conditional prefilling. We use LlamaGen-B as the generative model for experiments on ImageNet based on canny edge condition. In Fig. 2 (c), we depict the conditional consistency (F1-Score) and FID with respect to the number of training epochs for both approaches. Conditional decoding exhibits significant superiority over conditional prefilling in terms of both the speed of convergence and the final convergence result. Additionally, we provide a comparison of training resource consumption between the two approaches in Fig. 2 (d). Due to the substantial increase in the length of the sequence, conditional prefilling results in heightened memory consumption during training, as well as a notable decrease in training speed.

5 CONCLUSION

In this paper, we address autoregressive controllable image generation and present ControlAR, which allows autoregressive models to generate high-quality images according to diverse spatial controls. The proposed ControlAR encodes the spatial controls and adopts conditional decoding to superimpose control condition tokens on the image generation process. Moreover, ControlAR extends the capability of the autoregressive image generation model for arbitrary-resolution image generation. Experimental results under a variety of control conditions show that ControlAR is capable of precise control without compromising image quality, and is also very competitive with the diffusion model-based state-of-the-art methods.

REFERENCES

Holger Caesar, Jasper Uijlings, and Vittorio Ferrari. Coco-stuff: Thing and stuff classes in context. In *Proceedings of the IEEE conference on computer vision and pattern recognition*, pp. 1209–1218, 2018.

John Canny. A computational approach to edge detection. *IEEE Transactions on pattern analysis and machine intelligence*, (6):679–698, 1986.

Liang-Chieh Chen. Rethinking atrous convolution for semantic image segmentation. *arXiv preprint arXiv:1706.05587*, 2017.

Bowen Cheng, Ishan Misra, Alexander G Schwing, Alexander Kirillov, and Rohit Girdhar. Masked-attention mask transformer for universal image segmentation. In *Proceedings of the IEEE/CVF conference on computer vision and pattern recognition*, pp. 1290–1299, 2022.

Jia Deng, Wei Dong, Richard Socher, Li-Jia Li, Kai Li, and Li Fei-Fei. Imagenet: A large-scale hierarchical image database. In *2009 IEEE conference on computer vision and pattern recognition*, pp. 248–255. Ieee, 2009.

Prafulla Dhariwal and Alexander Nichol. Diffusion models beat gans on image synthesis. *Advances in neural information processing systems*, 34:8780–8794, 2021.

Alexey Dosovitskiy. An image is worth 16x16 words: Transformers for image recognition at scale. *arXiv preprint arXiv:2010.11929*, 2020.

Patrick Esser, Robin Rombach, and Bjorn Ommer. Taming transformers for high-resolution image synthesis. In *Proceedings of the IEEE/CVF conference on computer vision and pattern recognition*, pp. 12873–12883, 2021.

Patrick Esser, Sumith Kulal, Andreas Blattmann, Rahim Entezari, Jonas Müller, Harry Saini, Yam Levi, Dominik Lorenz, Axel Sauer, Frederic Boesel, et al. Scaling rectified flow transformers for high-resolution image synthesis. In *Forty-first International Conference on Machine Learning*, 2024.

Rinon Gal, Yuval Alaluf, Yuval Atzmon, Or Patashnik, Amit H Bermano, Gal Chechik, and Daniel Cohen-Or. An image is worth one word: Personalizing text-to-image generation using textual inversion. *arXiv preprint arXiv:2208.01618*, 2022.

Kaifeng Gao, Jiaxin Shi, Hanwang Zhang, Chunping Wang, and Jun Xiao. Vid-gpt: Introducing gpt-style autoregressive generation in video diffusion models. *arXiv preprint arXiv:2406.10981*, 2024.

Albert Gu and Tri Dao. Mamba: Linear-time sequence modeling with selective state spaces. *arXiv preprint arXiv:2312.00752*, 2023.

Kaiming He, Xiangyu Zhang, Shaoqing Ren, and Jian Sun. Deep residual learning for image recognition. In *Proceedings of the IEEE conference on computer vision and pattern recognition*, pp. 770–778, 2016.

Martin Heusel, Hubert Ramsauer, Thomas Unterthiner, Bernhard Nessler, and Sepp Hochreiter. Gans trained by a two time-scale update rule converge to a local nash equilibrium. *Advances in neural information processing systems*, 30, 2017.

Jonathan Ho, Ajay Jain, and Pieter Abbeel. Denoising diffusion probabilistic models. *Advances in neural information processing systems*, 33:6840–6851, 2020.

Jonathan Ho, Chitwan Saharia, William Chan, David J Fleet, Mohammad Norouzi, and Tim Salimans. Cascaded diffusion models for high fidelity image generation. *Journal of Machine Learning Research*, 23(47):1–33, 2022.

Edward J Hu, Yelong Shen, Phillip Wallis, Zeyuan Allen-Zhu, Yuanzhi Li, Shean Wang, Lu Wang, and Weizhu Chen. Lora: Low-rank adaptation of large language models. *arXiv preprint arXiv:2106.09685*, 2021.

Diederik P Kingma. Adam: A method for stochastic optimization. *arXiv preprint arXiv:1412.6980*, 2014.

Dan Kondratyuk, Lijun Yu, Xiuye Gu, José Lezama, Jonathan Huang, Grant Schindler, Rachel Hornung, Vighnesh Birodkar, Jimmy Yan, Ming-Chang Chiu, Krishna Somandepalli, Hassan Akbari, Yair Alon, Yong Cheng, Joshua V. Dillon, Agrim Gupta, Meera Hahn, Anja Hauth, David Hendon, Alonso Martinez, David Minnen, Mikhail Sirotenko, Kihyuk Sohn, Xuan Yang, Hartwig Adam, Ming-Hsuan Yang, Irfan Essa, Huisheng Wang, David A. Ross, Bryan Seybold, and Lu Jiang. Videopoet: A large language model for zero-shot video generation. In *Forty-first International Conference on Machine Learning, ICML 2024*, 2024.

Woosuk Kwon, Zhuohan Li, Siyuan Zhuang, Ying Sheng, Lianmin Zheng, Cody Hao Yu, Joseph Gonzalez, Hao Zhang, and Ion Stoica. Efficient memory management for large language model serving with pagedattention. In *Proceedings of the 29th Symposium on Operating Systems Principles*, pp. 611–626. ACM, 2023.

Haopeng Li, Jinyue Yang, Kexin Wang, Xuerui Qiu, Yuhong Chou, Xin Li, and Guoqi Li. Scalable autoregressive image generation with mamba. *arXiv preprint arXiv:2408.12245*, 2024a.

Ming Li, Taojiannan Yang, Huafeng Kuang, Jie Wu, Zhaoning Wang, Xuefeng Xiao, and Chen Chen. Controlnet++: Improving conditional controls with efficient consistency feedback. *arXiv preprint arXiv:2404.07987*, 2024b.

Xiang Li, Kai Qiu, Hao Chen, Jason Kuen, Zhe Lin, Rita Singh, and Bhiksha Raj. Controlvar: Exploring controllable visual autoregressive modeling. *arXiv preprint arXiv:2406.09750*, 2024c.

Yuheng Li, Haotian Liu, Qingyang Wu, Fangzhou Mu, Jianwei Yang, Jianfeng Gao, Chunyuan Li, and Yong Jae Lee. Gligen: Open-set grounded text-to-image generation. In *Proceedings of the IEEE/CVF Conference on Computer Vision and Pattern Recognition*, pp. 22511–22521, 2023.

Dongyang Liu, Shitian Zhao, Le Zhuo, Weifeng Lin, Yu Qiao, Hongsheng Li, and Peng Gao. Lumina-mgpt: Illuminate flexible photorealistic text-to-image generation with multimodal generative pretraining. *arXiv preprint arXiv:2408.02657*, 2024.

Cheng Lu, Yuhao Zhou, Fan Bao, Jianfei Chen, Chongxuan Li, and Jun Zhu. Dpm-solver: A fast ode solver for diffusion probabilistic model sampling in around 10 steps. *Advances in Neural Information Processing Systems*, 35:5775–5787, 2022.

Zhuoyan Luo, Fengyuan Shi, Yixiao Ge, Yujiu Yang, Limin Wang, and Ying Shan. Open-magvit2: An open-source project toward democratizing auto-regressive visual generation. *arXiv preprint arXiv:2409.04410*, 2024.

Chong Mou, Xintao Wang, Liangbin Xie, Yanze Wu, Jian Zhang, Zhongang Qi, and Ying Shan. T2i-adapter: Learning adapters to dig out more controllable ability for text-to-image diffusion models. In *Proceedings of the AAAI Conference on Artificial Intelligence*, volume 38, pp. 4296–4304, 2024.

Alex Nichol, Prafulla Dhariwal, Aditya Ramesh, Pranav Shyam, Pamela Mishkin, Bob McGrew, Ilya Sutskever, and Mark Chen. Glide: Towards photorealistic image generation and editing with text-guided diffusion models. *arXiv preprint arXiv:2112.10741*, 2021.

Maxime Oquab, Timothée Darcet, Théo Moutakanni, Huy Vo, Marc Szafraniec, Vasil Khalidov, Pierre Fernandez, Daniel Haziza, Francisco Massa, Alaaeldin El-Nouby, et al. Dinov2: Learning robust visual features without supervision. *arXiv preprint arXiv:2304.07193*, 2023.

William Peebles and Saining Xie. Scalable diffusion models with transformers. In *Proceedings of the IEEE/CVF International Conference on Computer Vision*, pp. 4195–4205, 2023.

Dustin Podell, Zion English, Kyle Lacey, Andreas Blattmann, Tim Dockhorn, Jonas Müller, Joe Penna, and Robin Rombach. Sdxl: Improving latent diffusion models for high-resolution image synthesis. *arXiv preprint arXiv:2307.01952*, 2023.

Reiner Pope, Sholto Douglas, Aakanksha Chowdhery, Jacob Devlin, James Bradbury, Jonathan Heek, Kefan Xiao, Shivani Agrawal, and Jeff Dean. Efficiently scaling transformer inference. In *Proceedings of the Sixth Conference on Machine Learning and Systems*. mlsys.org, 2023.

Can Qin, Ning Yu, Chen Xing, Shu Zhang, Zeyuan Chen, Stefano Ermon, Yun Fu, Caiming Xiong, and Ran Xu. Gluegen: Plug and play multi-modal encoders for x-to-image generation. In *Proceedings of the IEEE/CVF International Conference on Computer Vision*, pp. 23085–23096, 2023a.

Can Qin, Shu Zhang, Ning Yu, Yihao Feng, Xinyi Yang, Yingbo Zhou, Huan Wang, Juan Carlos Niebles, Caiming Xiong, Silvio Savarese, et al. Unicontrol: A unified diffusion model for controllable visual generation in the wild. *arXiv preprint arXiv:2305.11147*, 2023b.

Alec Radford, Jong Wook Kim, Chris Hallacy, Aditya Ramesh, Gabriel Goh, Sandhini Agarwal, Girish Sastry, Amanda Askell, Pamela Mishkin, Jack Clark, et al. Learning transferable visual models from natural language supervision. In *International conference on machine learning*, pp. 8748–8763. PMLR, 2021.

Colin Raffel, Noam Shazeer, Adam Roberts, Katherine Lee, Sharan Narang, Michael Matena, Yanqi Zhou, Wei Li, and Peter J Liu. Exploring the limits of transfer learning with a unified text-to-text transformer. *Journal of machine learning research*, 21(140):1–67, 2020.

Aditya Ramesh, Mikhail Pavlov, Gabriel Goh, Scott Gray, Chelsea Voss, Alec Radford, Mark Chen, and Ilya Sutskever. Zero-shot text-to-image generation. In *International conference on machine learning*, pp. 8821–8831. Pmlr, 2021.

René Ranftl, Katrin Lasinger, David Hafner, Konrad Schindler, and Vladlen Koltun. Towards robust monocular depth estimation: Mixing datasets for zero-shot cross-dataset transfer. *IEEE transactions on pattern analysis and machine intelligence*, 44(3):1623–1637, 2020.

Robin Rombach, Andreas Blattmann, Dominik Lorenz, Patrick Esser, and Björn Ommer. High-resolution image synthesis with latent diffusion models. In *Proceedings of the IEEE/CVF conference on computer vision and pattern recognition*, pp. 10684–10695, 2022.

Olaf Ronneberger, Philipp Fischer, and Thomas Brox. U-net: Convolutional networks for biomedical image segmentation. In *Medical image computing and computer-assisted intervention–MICCAI 2015: 18th international conference, Munich, Germany, October 5-9, 2015, proceedings, part III 18*, pp. 234–241. Springer, 2015.

Nataniel Ruiz, Yuanzhen Li, Varun Jampani, Yael Pritch, Michael Rubinstein, and Kfir Aberman. Dreambooth: Fine tuning text-to-image diffusion models for subject-driven generation. In *Proceedings of the IEEE/CVF conference on computer vision and pattern recognition*, pp. 22500–22510, 2023.

Chitwan Saharia, William Chan, Saurabh Saxena, Lala Li, Jay Whang, Emily L Denton, Kamyar Ghasemipour, Raphael Gontijo Lopes, Burcu Karagol Ayan, Tim Salimans, et al. Photorealistic text-to-image diffusion models with deep language understanding. *Advances in neural information processing systems*, 35:36479–36494, 2022.

Christoph Schuhmann, Romain Beaumont, Richard Vencu, Cade Gordon, Ross Wightman, Mehdi Cherti, Theo Coombes, Aarush Katta, Clayton Mullis, Mitchell Wortsman, et al. Laion-5b: An open large-scale dataset for training next generation image-text models. *Advances in Neural Information Processing Systems*, 35:25278–25294, 2022.

Jascha Sohl-Dickstein, Eric Weiss, Niru Maheswaranathan, and Surya Ganguli. Deep unsupervised learning using nonequilibrium thermodynamics. In *International conference on machine learning*, pp. 2256–2265. PMLR, 2015.

Jiaming Song, Chenlin Meng, and Stefano Ermon. Denoising diffusion implicit models. *arXiv preprint arXiv:2010.02502*, 2020a.

Yang Song and Stefano Ermon. Generative modeling by estimating gradients of the data distribution. *Advances in neural information processing systems*, 32, 2019.

Yang Song, Jascha Sohl-Dickstein, Diederik P Kingma, Abhishek Kumar, Stefano Ermon, and Ben Poole. Score-based generative modeling through stochastic differential equations. *arXiv preprint arXiv:2011.13456*, 2020b.

Peize Sun, Yi Jiang, Shoufa Chen, Shilong Zhang, Bingyue Peng, Ping Luo, and Zehuan Yuan. Autoregressive model beats diffusion: Llama for scalable image generation. *arXiv preprint arXiv:2406.06525*, 2024.

Keyu Tian, Yi Jiang, Zehuan Yuan, Bingyue Peng, and Liwei Wang. Visual autoregressive modeling: Scalable image generation via next-scale prediction. *arXiv preprint arXiv:2404.02905*, 2024.

Hugo Touvron, Thibaut Lavril, Gautier Izacard, Xavier Martinet, Marie-Anne Lachaux, Timothée Lacroix, Baptiste Rozière, Naman Goyal, Eric Hambro, Faisal Azhar, et al. Llama: Open and efficient foundation language models. *arXiv preprint arXiv:2302.13971*, 2023.

Aaron Van den Oord, Nal Kalchbrenner, Lasse Espeholt, Oriol Vinyals, Alex Graves, et al. Conditional image generation with pixelcnn decoders. *Advances in neural information processing systems*, 29, 2016.

Aäron Van Den Oord, Nal Kalchbrenner, and Koray Kavukcuoglu. Pixel recurrent neural networks. In *International conference on machine learning*, pp. 1747–1756. PMLR, 2016.

A Vaswani. Attention is all you need. *Advances in Neural Information Processing Systems*, 2017.

Jinheng Xie, Weijia Mao, Zechen Bai, David Junhao Zhang, Weihao Wang, Kevin Qinghong Lin, Yuchao Gu, Zhijie Chen, Zhenheng Yang, and Mike Zheng Shou. Show-o: One single transformer to unify multimodal understanding and generation. *arXiv preprint arXiv:2408.12528*, 2024.

Jiahui Yu, Yuanzhong Xu, Jing Yu Koh, Thang Luong, Gunjan Baid, Zirui Wang, Vijay Vasudevan, Alexander Ku, Yinfei Yang, Burcu Karagol Ayan, et al. Scaling autoregressive models for content-rich text-to-image generation. *arXiv preprint arXiv:2206.10789*, 2(3):5, 2022.

Lvmin Zhang, Anyi Rao, and Maneesh Agrawala. Adding conditional control to text-to-image diffusion models. In *Proceedings of the IEEE/CVF International Conference on Computer Vision*, pp. 3836–3847, 2023a.

Yuxin Zhang, Weiming Dong, Fan Tang, Nisha Huang, Haibin Huang, Chongyang Ma, Tong-Yee Lee, Oliver Deussen, and Changsheng Xu. Prospect: Prompt spectrum for attribute-aware personalization of diffusion models. *ACM Transactions on Graphics (TOG)*, 42(6):1–14, 2023b.

Shihao Zhao, Dongdong Chen, Yen-Chun Chen, Jianmin Bao, Shaozhe Hao, Lu Yuan, and Kwan-Yee K Wong. Uni-controlnet: All-in-one control to text-to-image diffusion models. *Advances in Neural Information Processing Systems*, 36, 2024.

Bolei Zhou, Hang Zhao, Xavier Puig, Sanja Fidler, Adela Barriuso, and Antonio Torralba. Scene parsing through ade20k dataset. In *Proceedings of the IEEE conference on computer vision and pattern recognition*, pp. 633–641, 2017.

Chunting Zhou, Lili Yu, Arun Babu, Kushal Tirumala, Michihiro Yasunaga, Leonid Shamis, Jacob Kahn, Xuezhe Ma, Luke Zettlemoyer, and Omer Levy. Transfusion: Predict the next token and diffuse images with one multi-modal model. *arXiv preprint arXiv:2408.11039*, 2024.

Deyao Zhu, Jun Chen, Xiaoqian Shen, Xiang Li, and Mohamed Elhoseiny. Minigpt-4: En-hancing vision-language understanding with advanced large language models. *arXiv preprint arXiv:2304.10592*, 2023.

A APPENDIX

A.1 IMPLEMENTATION DETAILS

Dataset details. The quantity of images from all datasets utilized in our experiment is detailed in Tab. 7. We utilize the ImageNet-1K (Deng et al., 2009) as the training dataset for class-to-image controllable generation, encompassing a total of 1,000 classes. The canny edge detector (Canny, 1986) is employed to acquire the canny edge map, and the depth map is obtained using Midas (Ranftl et al., 2020). In the context of text-to-image controllable generation, ADE20K (Zhou et al., 2017) and COCOStuff (Caesar et al., 2018) are harnessed for training the segmentation control task, while MultiGen-20M is utilized for training the edge map and depth control generation.

Table 7: **Details of different dataset.**

	ImageNet-1K	ADE20K	COCOStuff	MultiGen-20M
Training Samples	1281188	20210	118287	2810616
Evaluation Samples	50000	2000	5000	5000

Evaluation details. To assess the conditional consistency of the generated images, we have de-vised various metrics tailored to each specific task. In the context of segmentation control gener-ation, we employ a segmentation model to evaluate the mean Intersection over Union (mIoU) of the generated images. Specifically, we reference ControlNet++ to examine the results of the valida-tion set generation on ADE20K using Mask2Former (Cheng et al., 2022), and on COCOStuff using DeepLabv3 (Chen, 2017). For canny edge control generation, we utilize the canny edge detector with thresholds of (100, 200) to derive the canny edge of the results, and subsequently calculate the F1-Score in relation to the input control. In the case of hed and lineart edge, we follow the approach outlined in ControlNet to obtain control images and compute the Structural Similarity Index (SSIM). Regarding depth map control generation, we calculate the Root Mean Square Error (RMSE).

Table 8: **Training details of different tasks.**

	Seg.		Canny	Hed	Lineart	Depth
	ADE20K	COCOStuff		MultiGen-20M		
Batch size	96	96	96	88	88	96
GPU hours	55	80	340	160	110	370

Training details. We use 8 Nvidia A100 80G GPUs to complete text-to-image controllable gener-ation experiments based on LlamaGen-XL (Sun et al., 2024). The batch size settings and GPU hours during training can be found in Tab. 8. We use the edge extraction model to obtain the hed edge and lineart edge of the image during the training process, which takes up some memory, so the batch size is slightly smaller than the other tasks. It should be noted that since the ADE20K dataset has less training data, we first merge the ADE20K and COCOStuff datasets together to train the model, which requires roughly 50 GPU hours. Because the segmentation map labelling is inconsistent be-tween the two datasets, we fine-tuned 2k iterations on ADE20K and 20k iterations on COCOStuff, respectively. The additional 2k iteration on ADE20K results in a mIoU improvement of 1.15.

A.2 DISCUSSION

Limitation. We have shown in our experiments that updating the parameters of the generative model can achieve better results than freezing it completely. However, this approach is still not as convenient as ControlNet in terms of model portability. In addition, our method does not currently support scenarios where multiple control images are input simultaneously. Processing multiple control images simultaneously using a control encoder with a small number of parameters can be challenging.

Future work. We will use more data to try more kinds of conditional control generation, such as human pose and bounding box. At the same time, in order to improve the migratability of the model we will consider focusing the parameter update on the control encoder and keep the parameters of the generated model itself unchanged. In addition to this, how to use one control encoder to process different control image inputs simultaneously is also a direction worth exploring.

A.3 MORE VISUALIZATIONS

More visualization results under different conditions of control are shown in Fig. 7 8 9 10 11. We alse show some visualization comparison of ControlAR and MR-ControlAR at different resolution in Fig. 12 and Fig. 13.

Condition   Generated Images

Figure 7: **Segmentation mask control generation visualization.**

Condition   Generated Images

Figure 8: **Canny edge control generation visualization.**

Condition   Generated Images

Figure 9: **Hed edge control generation visualization.**

Condition   Generated Images
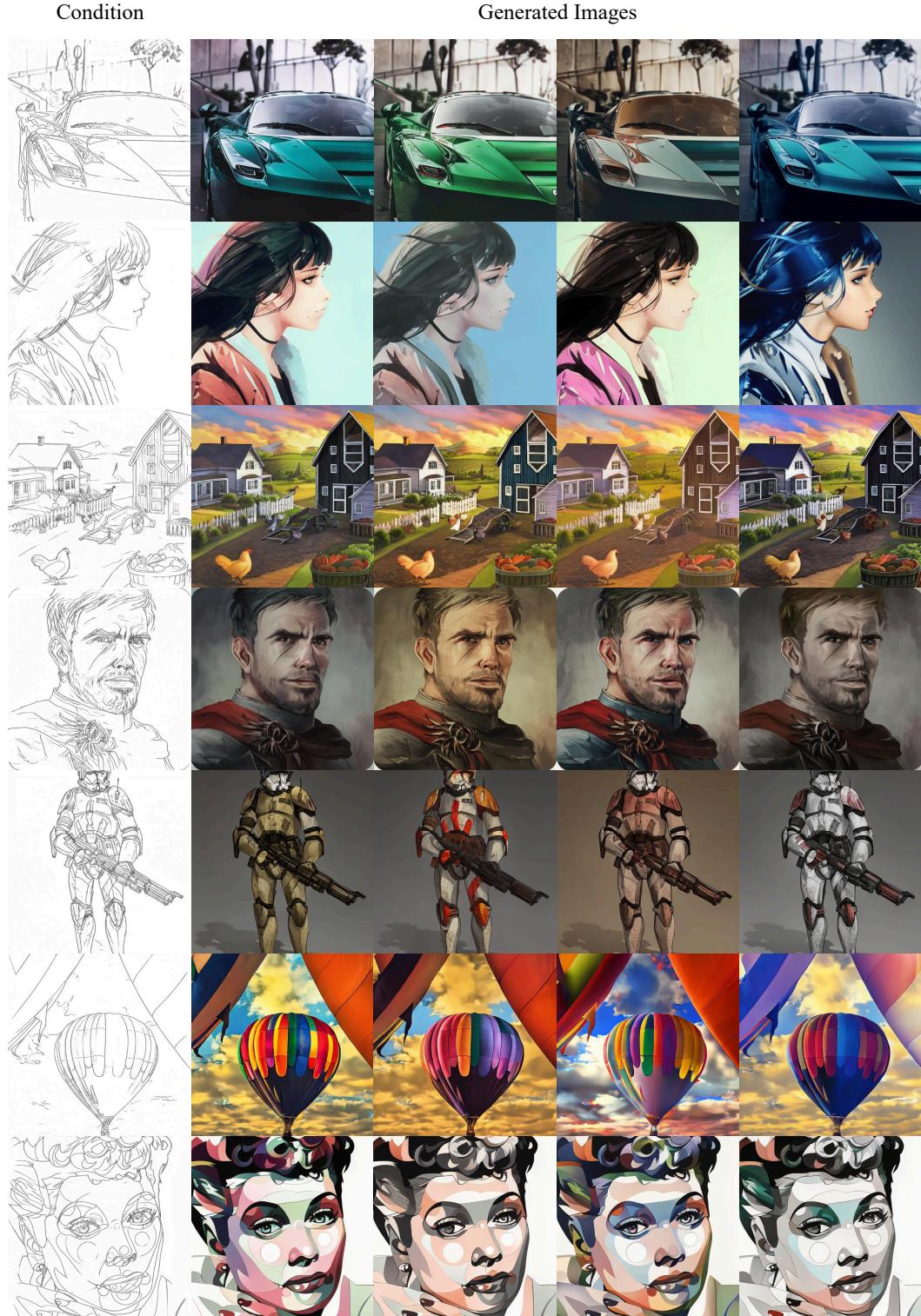
Figure 10: **Lineart edge control generation visualization.**

Condition   Generated Images
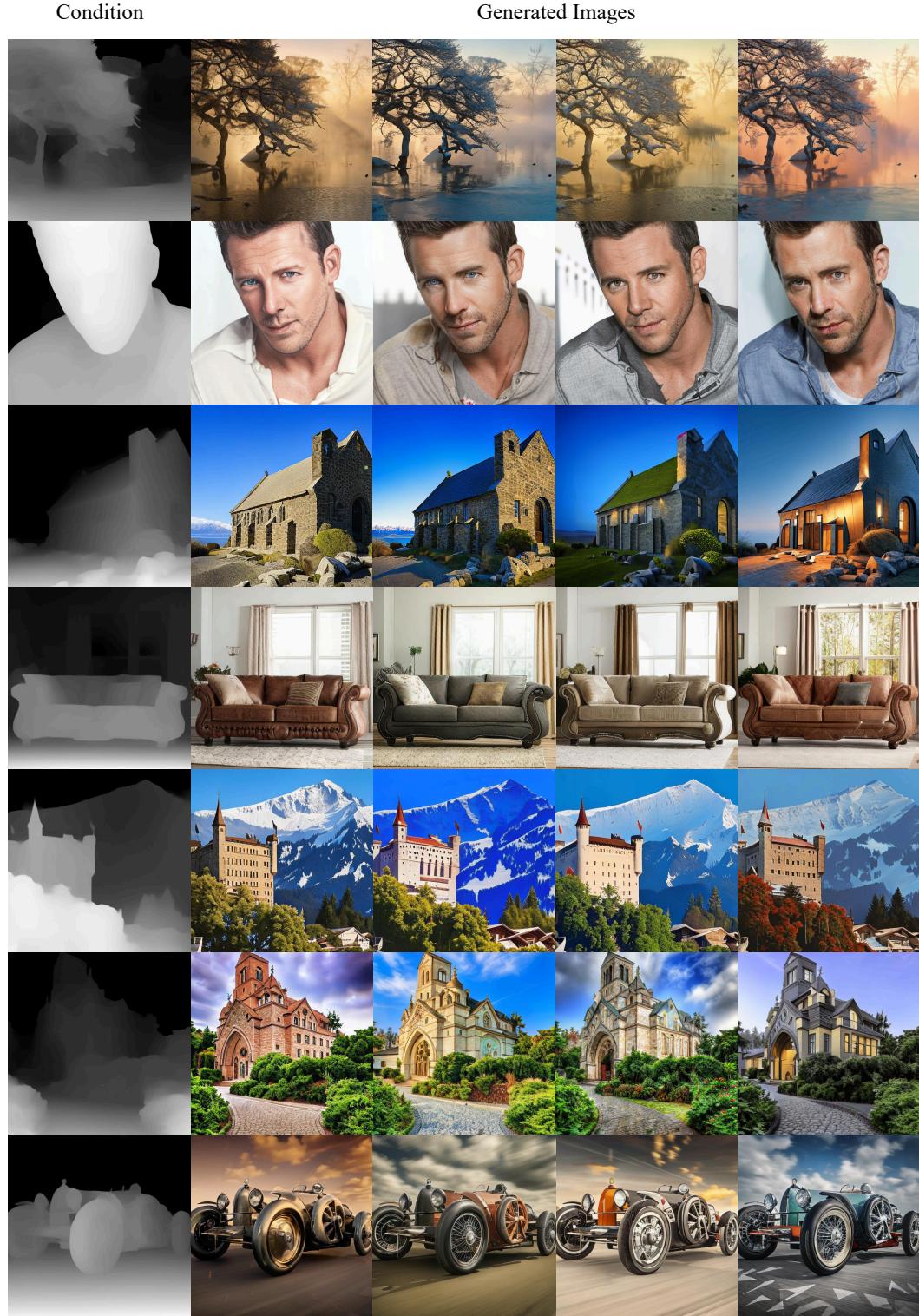
Figure 11: **Depth map control generation visualization.**
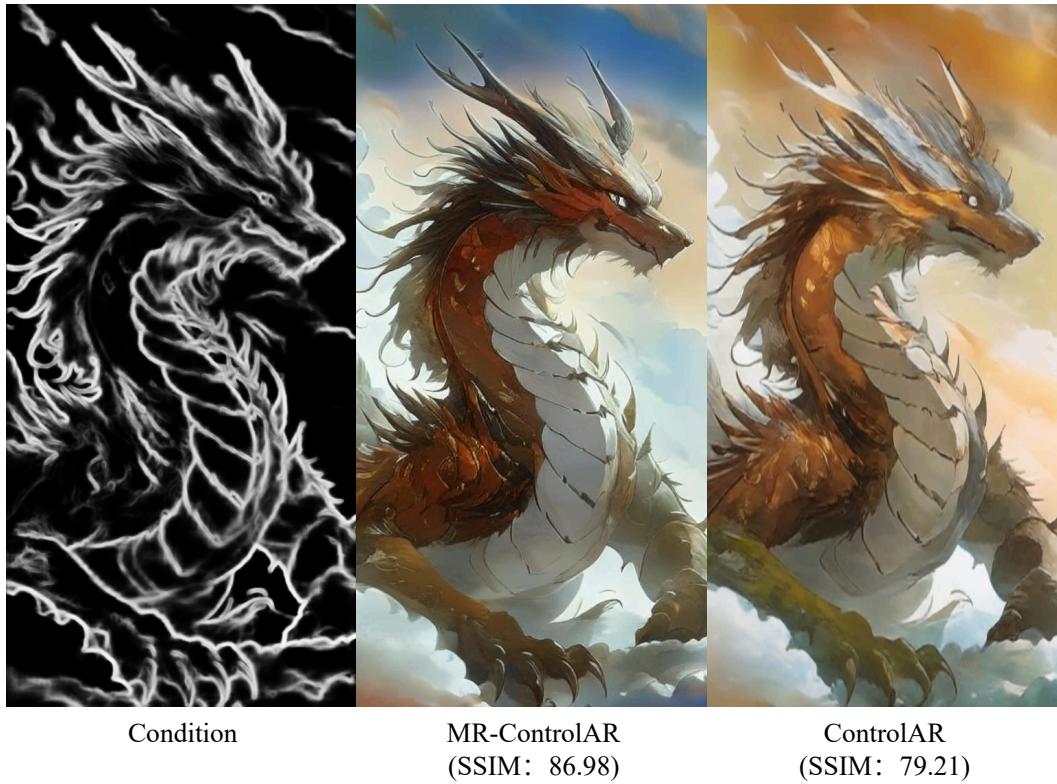
| Condition | MR-ControlAR
(SSIM: 86.98) | ControlAR
(SSIM: 79.21) |

Figure 12: **visualization comparison of MR-ControlAR and ControlAR at the resolution of** 1024×512**.**

Condition
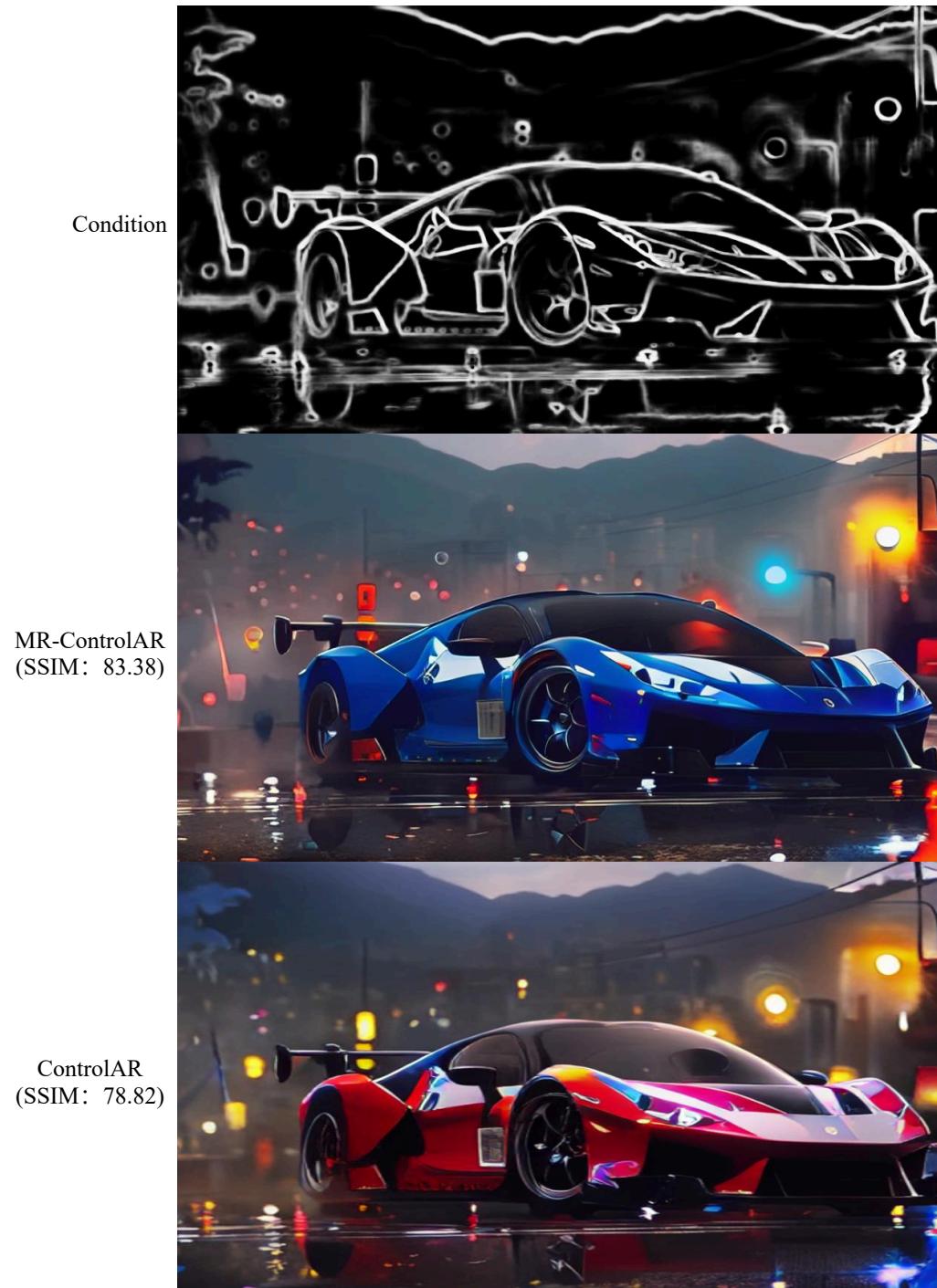
MR-ControlAR
(SSIM：83.38)

ControlAR
(SSIM：78.82)

Figure 13: **visualization comparison of MR-ControlAR and ControlAR at the resolution of** 576×1024**.**